HHS Public Access

Author manuscript

Ocul Surf. Author manuscript; available in PMC 2023 July 01.

Published in final edited form as:

Ocul Surf. 2022 July ; 25: 8–18. doi:10.1016/j.jtos.2022.03.006.

Optical Coherence Tomography Angiography in the Evaluation of Vascular Patterns of Ocular Surface Squamous Neoplasia During Topical Medical Treatment

Despoina Theotoka, MD, MSc[1,3,*], **Zhiping Liu, MD, PhD**[1,4,*], **Sarah Wall, MD**[1,3], **Anat Galor, MD**[1,2], **Ghada J. Al Bayyat, MD**[1], **William Feuer, MS**[1], **Jianhua Wang, MD, PhD**[1], **Carol L. Karp, MD**[1,#]

[1]Department of Ophthalmology, Bascom Palmer Eye Institute, University of Miami Miller School of Medicine, Miami, USA

[2]Department of Ophthalmology, Miami Veterans Administration Medical Center, Miami, FL, USA

[3]Department of Ophthalmology and Visual Science, Yale School of Medicine, New Haven, Connecticut

[4]Ophthalmic Center, the Second Affiliated Hospital of Guangzhou Medical University, Guangzhou, Guangdong, China

Abstract

Purpose: Optical coherence tomography angiography (OCTA) was utilized to examine changes in ocular surface squamous neoplasia (OSSN) vascular patterns over time in individuals treated with topical medical therapy.

Methods: Ten individuals with OSSN diagnosed by clinical examination and high resolution (HR)-optical coherence tomography (OCT) were recruited. All individuals received topical immuno- or chemotherapy. OCTA images were obtained and analyzed at three points: presentation, mid-treatment and tumor resolution. Tumor metrics including tumor area (TA), tumor volume (TV), tumor depth (TD), and total tumor density (TTD) were calculated. Vessel area density (VAD) was also quantified within the OSSN, the subepithelium under and adjacent to the OSSN and the subepithelium of the uninvolved, contralateral eye. Vascular network changes were also subjectively evaluated.

Results: TA, TV, TD and TTD all significantly decreased with time ($p<0.001$). The mean VAD within the OSSN significantly decreased ($p<0.001$) between visits (presentation: 26.52±6.8%, mid-treatment: 7.19±5.88%, tumor resolution: 0.11±0.34%). The mean subepithelial VAD under

[#]**Correspondence:** ckarp@med.miami.edu; Bascom Palmer Eye Institute, University of Miami Miller School of Medicine, 900 NW 17th Street, Miami, FL 33136, USA.

[*]These two authors contributed equally and should be considered as co-first authors.

5. Disclosure/Conflict of Interest Statement:
The authors have no financial disclosures that would be a potential conflict of interest.

the OSSN also decreased with time (23.22±11.03%, 20.99±5.99% and 19.58±7.08%), and after resolution the sub-tumor VAD (19.58±7.08%) was comparable to the subepithelial VAD in the contralateral eye (15.47±4.37%, p>0.05). The mean VAD in the subepithelium adjacent to the OSSN increased with treatment, then decreased significantly between mid-treatment and resolution (23.26±4.54, 28.30±7.43% and 21.68±6.10%, p=0.009). Qualitatively, the tumor subepithelial vascular network was complex and dense but with tumor resolution appeared less tortuous and similar to the uninvolved eye.

Conclusion: OCTA provided insight into the pathophysiology of tumor angiogenesis, showing decreased vascular density and normalization of vascular networks associated with tumor resolution.

Keywords

ocular surface squamous neoplasia; OSSN; vascular networks; vessel area density; optical coherence tomography angiography; OCTA; 5-fluorouracil; Interferon α-2b

1. Introduction

The term ocular surface squamous neoplasia (OSSN), first described by Lee and Hirst in 1995 (1), encompasses a spectrum of neoplastic changes in the squamous epithelium of the cornea and conjunctiva ranging from dysplasia to invasive squamous cell carcinoma (SCC). OSSN was found to be the most common non-pigmented conjunctival tumor in a retrospective study of 2412 conjunctival lesions, in which 29% (n=716) of the lesions were pre-malignant or malignant squamous epithelial neoplasms. (2) Treatment modalities for OSSN include wide surgical excision and intraoperative cryotherapy, topical immuno- and chemotherapy such as 5- fluorouracil (5-FU), interferon α-2b (IFN α-2b) and mitomycin C (MMC) or a combination of surgical and medical treatment. (3) Topical medical treatment has recently become the treatment of choice especially in diffuse or multifocal lesions as it has the advantage of treating the entire ocular surface and avoid scarring. (4)

The clinical appearance of OSSN varies and it can appear as a flat or elevated lesion. It may present as a gelatinous, leukoplakic, papillary or opalescent lesion. It is mostly commonly at the limbus and is often accompanied by abnormal vessels (hairpin or prominent feeder vessels). (3, 5) Although histopathologic analysis remains the gold-standard for diagnosis, high resolution optical coherence tomography (HR-OCT) has proven to be a valuable tool in the diagnosis of OSSN. The characteristic findings of OSSN on HR-OCT include a thickened, hyperreflective epithelium with an abrupt transition of the abnormal to the normal epithelium. (6) HR-OCT can also assist in disease management as clinical progression or regression of the tumor can be identified and treatment may be adjusted accordingly. (7) For example, HR-OCT may reveal subtle epithelial thickening which cannot be visualized clinically, preventing premature termination of treatment. (8) However, HR-OCT is not able to visualize angiographic characteristics of OSSN.

OCT angiography (OCTA) is a novel diagnostic method that has emerged as an important tool for imaging ocular vascular patterns. Compared to fluorescein angiography (FA) and indocyanine green angiography (ICGA) (9, 10), OCTA is less invasive and comes without

the risks associated with the use of dyes (e.g., anaphylaxis; contraindications with pregnancy and liver or kidney disease). While OCTA technology has mostly been applied to the posterior segment of the eye, there is increasing research on the use of OCTA for imaging the anterior segment (11), with several studies describing vascular patterns in the cornea, conjunctiva, sclera and iris. (11-13)

OCTA has only recently been applied to the study of OSSN. We previously characterized the morphology of vascular patterns in OSSN through OCTA prior to any treatment. We found that tumor vascular networks which were not visualized clinically were identified by OCTA. (14) In this paper, we further investigate how these vascular patterns change with medical treatment for OSSN.

2. Methods

2.1 Study design, setting, and population

Thirty individuals with a new diagnosis of OSSN were prospectively recruited from the Bascom Palmer Eye Institute, University of Miami Miller School of Medicine between November 2018 and July 2020. A complete ocular examination was performed on all patients in our ocular surface oncology clinic and the diagnosis of OSSN was established through clinical and HR-OCT presentation. Biopsy was deliberately not performed in order to preserve the original vascular patterns within and surrounding the tumor. Subjects were medically treated with topical 5-FU 1% (4 times daily for 1 week, followed by 3 weeks of drug holiday), IFN α-2b (1 million IU/ml (MIU/ml) 4 times daily without holiday), or MMC (0.04%, 4 times daily for 1 week, followed by 2-3 weeks of drug holiday). Subjects were evaluated every 2 months and at each visit, a complete ocular examination, slit-lamp photograph, HR-OCT, and OCTA were performed. The treatment regimen was continued until the tumor was deemed resolved by clinical exam and HR-OCT imaging. The criterion for clinical resolution was slit-lamp examination revealing resolution of the OSSN lesion and its associated abnormal blood vessels. The criteria for OCT resolution were (1) normalization of epithelial thickness (2) no longer abrupt transition from normal to abnormal epithelium, and (3) resolution of epithelial hyper-reflectivity.

Demographics, medical history and medication information were collected from the patients' medical records. This study was approved by the Institutional Review Board of the University of Miami, Miller School of Medicine and was conducted in accordance with the principles of Declaration of Helsinki. Written informed consent was obtained from all participants.

2.2 Tumor characteristics

An ocular surface oncology expert (CLK) examined all patients. The diagnosis of OSSN was made based on clinical examination, slit-lamp photographs and anterior segment HR-OCT findings. The appearance of the tumor (leukoplakic, papillary and/or gelatinous, flat or raised, localized or diffuse), as well as the location described in the context of clock hours were documented in all cases. All lesions were stained with rose bengal or lissamine green to evaluate for the presence of devitalized cells. The classic characteristics of OSSN

on HR-OCT, thickened, hyperreflective epithelium with an abrupt transition of the normal from the abnormal epithelium (3, 6-8) were identified and documented in all individuals as well. Clinical and HR-OCT tumor characteristics were documented in the same manner on all follow-up visits.

2.3 Anterior segment optical coherence tomography angiography examination

The Optovue OCTA device (Optovue, Fremont, CA, USA) mounted with an adaptor lens for the anterior segment (CAM-L, Optovue) was utilized to acquire anterior segment angiography images. The device performs 70,000 A-scans every second with an 840 nm central wavelength, a 5 μm resolution, and a 22 μm beamwidth. Each scan of anterior segment angiography included a raster scan with 304 (A-scan) x 304 (B-scan). As reported previously (14, 15), the angiography dataset of 6 × 6 mm scan pattern with a field of view (FOV) of 8.775 × 8.775 mm was utilized. OCTA was performed by the same well-trained technician until high-quality images were obtained and quantification was performed twice by the same observer. Poor quality images were excluded from the analysis.

2.4 Location and timing of image acquisition

An image of the entire tumor was obtained. The central area was defined as the geometric center of the tumor. The peripheral area was defined as an area of 2.14 mm^2 at the conjunctival border of the tumor, in an area where the tumor thickness measured less than 300 μm. In our previous work (16) we demonstrated that blood flow signals in layers deep to the tumor were diminished in tumors with thickness more than 300 μm, leading to inaccurate VAD measurements. This was especially important for analyzing the subepithelial layers as shadowing from the overlying tumor made it even more challenging to measure the subepithelial blood vessels. As such, VAD was measured in peripheral areas of the tumor to avoid blockage and false negative density evaluation.

Thus, three different areas were analyzed at every visit.

1. The epithelium within the tumor at the tumor edge
2. The subepithelial tissue under the tumor epithelium at the tumor edge (200 μm)
3. The subepithelial tissue adjacent to the tumor (200 μm)

In addition, the subepithelial tissue was analyzed in the contralateral, uninvolved eye in a mirrored area.

For the analysis, three different time points were examined: presentation prior to treatment initiation, mid-treatment, and tumor resolution. The contralateral, uninvolved eye was analyzed at presentation only. Mid-treatment was defined as a point in time during topical chemotherapy in which tumor was reduced in size but still present. Tumor resolution was based on clinical resolution as seen on slit-lamp examination as well as findings on HR-OCT images.

2.5 Image segmentation and quantitative analysis

All ROI were segmented using a commercial software program (OrionTM, Voxeleron LLC, Pleasanton, CA, USA). The volumetric OCTA data were analyzed using the software utility provided by the OCTA manufacturer. The dataset containing the OCT structure and angiography data was exported and loaded into the Orion software, which was utilized to perform manual segmentations of the volumetric OCTA data. During image processing, enface and cross-sectional images of the OSSN were analyzed, first outlining the area and the depth of the lesion. The superficial and deep boundaries of conjunctival and/or corneal tumor were outlined in the cross-sectional image. Subepithelial tissue, 200 μm underneath the inferior boundary of OSSN, was also outlined. That cutoff was selected based on the rationale that the area underneath 200 μm may contain vessels from the sclera which might alter the vascular density calculations. Similarly, the epithelium and sub-epithelial tissue (200 μm) immediately adjacent to the OSSN were delineated. In the contralateral, unaffected eye, the area mirroring the area of the tumor in the affected eye was analyzed; the superficial and deep boundaries of the epithelium were outlined and the subepithelial tissue 200 μm underneath the inferior boundary of the epithelium was also outlined.

Then, the enface vessel images of the epithelial and the subepithelial segmented tissue were exported. A region of interest (ROI) was selected in the peripheral area along the edge of the conjunctival component of the tumor. Then the vessels were analyzed in that ROI (1 × 1 mm in the Orion Software). This resulted in an area of 1.463 × 1.463 mm (2.14 mm^2) due to the magnification effect of the CAM-L anterior segment lens attached to the OCTA. This was the same for all subjects. After cropping the enface images of the segmented tissue, the ROI had specific coordinates.

Photoshop (Adobe, San Jose, CA, USA) was used for image editing and equalization and image conversion to a grayscale mode was performed. In addition, projection artifacts were removed by applying the subtract blend mode to subtract the vessel image of the superficial layer (tumor or epithelium) from the deep layer. Image J (NIH Bethesda, Maryland, USA) was used for further processing of the grayscale image. To generate the binary image, a series of filtering and thresholding, involving Gaussian blurring (Sigma = 4), bandpass filtering, and Otsu's Thresholding were utilized.

Vessel area density (VAD) within the binary images was calculated as the ratio of the area (ROI) occupied by the vessels per unit area as described previously (14, 15). We measured VAD in three locations: the epithelium within the tumor at the tumor edge (where the tumor was less than 300 μm in thickness), the subepithelial tissue under the tumor epithelium at the tumor edge and the adjacent uninvolved subepithelial tissue (200 μm). We measured the subepithelial VAD of the contralateral, unaffected eye in a mirroring location. In addition, we measured the total visible vascular density of the entire tumor epithelium which was named total tumor density (TTD). Other metrics evaluated included tumor area, tumor volume and tumor depth. Tumor area and tumor volume were automatically calculated through the Orion software while tumor depth was calculated through the following formula tumor volume /tumor area* 1000. Additionally, the vascular network was evaluated subjectively through visual evaluation. Vascular features, including the presence of feeder

and hairpin vessels were examined on all OCTA images. All measurements were performed twice by one observer.

The analysis was performed in the same way for images of the contralateral unaffected eye and for images of subsequent visits. The same location of cornea/conjunctiva as the original tumor location was imaged in the affected eye and in the fellow eye over time. The area for vessel calculation matched the area of the eye with the tumor, based on the ROI coordinates. Anatomical landmarks were also used to help ensure the area mirrored the original tumor location.

2.6 Statistical analysis

IBM SPSS Statistics software package (version 25, IBM Corp., Armonk, NY, USA) was utilized for the statistical analysis. All values are presented as mean ± standard deviation. Descriptive statistics were used to summarize patient demographic and clinical information. The measured metrics were VAD (presented as mean ± standard deviation, %), tumor area (measured in mm2), tumor volume (measured in mm3), tumor depth (measured in μm), and total tumor density (presented as mean ± standard deviation, %), which were measured at the different locations mentioned above and compared at 3 time points. We used parametric tests to analyze VAD parameters and we did not perform Bonferroni correction for multiple tests, as this methodology has its own limitation. (17) Generalized estimating equation (GEE) was used to determine significance of change over time. The main outcome variable was VAD which was compared between the different points in time. Paired t tests were used to compare mean differences in VAD between the involved and uninvolved (contralateral) eye. Relationships between baseline VAD of epithelial and sub-epithelial under and adjacent to the tumor and change in VAD (presentation-resolution) were examined with respect to months to clinical resolution using Pearson correlational analyses.

Vessel patterns were also qualitatively described and compared to clinical tumor appearance during treatment. P value less than 0.05 was considered statistically significant.

3. Results

3.1 Patient population

Of 30 individuals, 10 had high-quality OCTA images suitable for analysis at all 3 time points. The mean age of the 10 individuals was 61.4± 15 years, 70% were male, all were white, 50% self-identified as Hispanic (Table 1).

3.2 Timeline

Due to variability in follow up and tumor response, the mid-treatment time point varied, with 6 lesions measured 2 months after initiation of topical medical therapy, 3 lesions measured at 4 months and 1 lesion at 6 months. Time to tumor resolution from initiation of therapy ranged from 6 to 13 months with an average of 9 months. We did not observe tumor recurrence after completion of topical medical treatment in the ten individuals.

3.3 Analysis of the angiography images

Quantitative analysis of images in all 10 individuals was performed at the 3 times points. The mean tumor area, tumor volume, tumor depth, and total tumor density were found to be 29.59±9.48 mm^2, 9.05±3.43 mm^3, 318±117 μm and 33.49±11.12% at presentation (n=10), 11.37±7.34 mm^2, 2.69±2.37 mm^3, 204±78 μm and 5.32±3.07% at mid-treatment (n=6 for tumor area, tumor volume, tumor depth and n=4 for total tumor density) and zero at tumor resolution, statistically decreasing between all visits ($p<0.001$), (Figure 1). In four cases, the tumor was too small to be accurately measured through the Orion software (unable to measure tumor area, tumor volume, tumor depth, and total tumor density) and in two cases keratinization prevented quantification of total tumor density.

The mean VAD in the tumor epithelium significantly decreased over time: 26.52±6.8% at presentation, 7.19±5.88% at mid-treatment and 0.11±0.34% at tumor resolution ($p<0.001$), (Figure 2). The mean VAD in the subepithelial space immediately beneath the tumor (200 μm) also decreased overtime: 23.22±11.03% at presentation, 20.99±5.99% at mid-treatment and 19.58±7.08% at tumor resolution (Figure 2), however this change was not significant. The subepithelial VAD under the tumor at tumor resolution (19.58±7.08%) was similar to values obtained in the contralateral healthy eye at the same location (15.47±4.37%, $p>0.05$). The mean VAD in the subepithelial tissue (200 μm) adjacent to the OSSN first increased from presentation to mid-treatment, then decreased from midpoint to tumor resolution (23.26±4.54% at presentation, 28.30±7.43% at mid-treatment, and 21.68±6.10% at tumor resolution, $p=0.009$ between mid-treatment and tumor resolution), (Figure 2). Figure 3 and Figure 4 demonstrate the noted observation that blood vessel density in the subepithelial tissue adjacent to the neoplastic epithelium first increased and then subsequently decreased. We observed statistically significant correlations between baseline subepithelial VAD adjacent to the tumor and change in subepithelial VAD adjacent to the tumor (presentation-resolution) and months to clinical resolution ($p<0.05$ for both, pearson correlation=0.733 and 0.696 respectively).

Qualitatively, the tumor vascular network was noted to be irregular, complex and dense at presentation. This chaotic vascular network was noted within the epithelial tumor as well as in the subepithelial tissue immediately beneath and adjacent to the epithelial tumor. In particular, the two tumors with papillomatous features (Figures 3 and 6) exhibited a “sea fan” pattern of blood vessels. This chaotic tumor vascular network gradually disappeared in the epithelium as the tumor regressed. The blood vessels in the area immediately beneath and adjacent to the epithelial tumor slowly demonstrated a more regular appearance as the tumor was treated and ultimately looked similar to the contralateral unaffected eye. On OCTA, we identified vascular trunks which appeared larger in diameter and traveled towards the lesion which may represent feeder vessels. At presentation, 9 of 10 lesions had hairpin vessels visible on OCTA images which regressed in all cases with treatment. Larger vessels which may represent feeder vessels, were visible on OCTA images in 8 of the 10 lesions at presentation, which also all regressed with treatment.

When looking at the control location, no blood vessels were seen in the epithelium of the contralateral, unaffected eye. After tumor resolution, the subepithelial VAD in the location

of tumor (VAD=19.57%) was similar to the subepithelial VAD in the control location (VAD=15.47%), p=0.62.

Selective cases demonstrating qualitative changes in vascular network patterns with chemotherapy—As described above, tumor metrics including tumor area, tumor volume, tumor depth and total tumor density significantly decreased with treatment and were not quantifiable upon tumor resolution in all cases. ($p<0.001$) Not surprisingly, VAD within the OSSN also significantly decreased with treatment and it was calculated as almost zero with tumor resolution. ($p<0.001$) When looking at individual cases, they all followed this significant pattern.

Concerning VAD in the subepithelial tissue adjacent to the OSSN, we expected levels to decrease at each timepoint since the tumor gradually decreased in size in all cases, however more variation was noted in the VAD. The *mean* VAD in the subepithelial tissue adjacent to the OSSN actually increased before decreasing (minimum change to classify cases as increased or decreased was that of 1 point). Interestingly, when analyzing on a case-by-case basis, VAD levels notably increased in mid-treatment in 50% (5/10) of cases, remained stable in 10% (1/10) of cases and decreased in 40% (4/10) of cases, however that decrease was of a smaller amplitude. With continued treatment and subsequent tumor resolution, VAD decreased in 50% (5/10) of cases, remained stable in 40% (4/10) of cases and marginally increased in 10% (1/10) of cases. We did notice statistically significant correlations between baseline and change (presentation-resolution) in subepithelial VAD adjacent to the tumor and months to clinical resolution ($p<0.05$ for both, Pearson correlation=0.733 and 0.696 respectively).

Furthermore, we measured VAD in the subepithelial tissue under the tumor. Although the *mean* VAD in the subepithelial tissue under the tumor decreased between visits, VAD levels directly under the tumor exhibited the highest variation when looking at individual cases. This was likely due to tumor thickness and leukoplakia which precluded clear visualization of the underlying subepithelial vascular plexus in some cases, and thus underestimating the VAD due to blockage by the tumor.

Some select cases are described below:

Case 1 highlighting an increase in the adjacent subepithelial vascular plexus at mid-treatment with subsequent decrease at tumor resolution.: A 38-year-old male presented with an OSSN with a leukoplakic edge and a papillomatous base encroaching on the cornea nasally from 2 to 4 o'clock in the right eye. (Figure 3). It was characterized clinically by prominent vascularity within the tumor and multiple feeder vessels. HR-OCT confirmed the presence of a thickened, hyperreflective epithelium with abrupt transition from the normal epithelium. The head of the tumor was especially thick and leukoplakic as seen in HR-OCT and in the thickness map. Posterior shadowing was present under the thicker parts of the tumor. En face angiography imaging revealed a dense vascular network within the papillomatous portion/tail of the OSSN peripherally and in the adjacent underlying subepithelial tissue. No blood vessels were seen within the tumor head (asterisk) as they

were blocked by the leukoplakia. Throughout treatment, the tumor area, tumor volume, tumor volume, tumor depth, and total tumor density all decreased.

When evaluating VAD at presentation, the leukoplakia prevented visualization of blood vessels at that corresponding part of the tumor and the respective subepithelial tissue. Nevertheless, VAD in the epithelium and the subepithelial tissue was measured at the non-leukoplakic part of the tumor. At mid-treatment, post 2 cycles of 5-FU and 3 cycles of MMC, the OSSN had shrunk remarkably. The leukoplakic component of the OSSN resolved while some papillomatous component remained. HR-OCT confirmed the presence of a small residual tumor. This was dramatically decreased in thickness when comparing with presentation. As the lesion decreased in size, vessels in the tumor tail were resolved, however a “sea-fan” vascular pattern was visualized within the remaining papillomatous tumor head (white arrow). At tumor resolution, post 2 additional cycles of MMC, the OSSN was resolved on slit-lamp and HR-OCT imaging. En face angiography showed a grossly avascular epithelium while the subepithelial vascular network appeared to have normalized.

During the course of the treatment, the tumor area, tumor volume, tumor volume, tumor depth, and total tumor density decreased with treatment and eventually were calculated as zero with tumor resolution. As expected, VAD within the OSSN greatly decreased and eventually approached zero with tumor resolution. Most interestingly, the VAD in the subepithelial tissue adjacent to the OSSN increased in mid-treatment (arrowheads) before decreasing with tumor resolution. VAD in the subepithelial tissue under the OSSN at the non-leukoplakic tumor edge decreased in mid-treatment and then further decreased with tumor resolution. At resolution, the VAD in the subepithelial tissue below the tumor (19.56%) was comparable to subepithelial VAD in the contralateral uninvolved eye in a similar location (15.13%). (Figure 3).

Case 3 highlighting an increase in the adjacent subepithelial vascular plexus at mid-treatment with subsequent decrease at tumor resolution.: A 60-year-old woman presented with corneal and limbal gelatinous OSSN in the left eye nasally from 6 to 12 o’clock. (Figure 4). HR-OCT confirmed the presence of a thickened, hyperreflective epithelium with abrupt transition from the normal epithelium. En face angiography imaging showed a vascular network within the tumor and a rich vascular network underneath the tumor.

At mid-treatment, after 4 cycles of 5-FU, the tumor was dramatically improved clinically, but some opalescence and gelatinous changes persisted around 8 to 9 o’clock. By OCTA, the internal tumor vascular network appeared mostly resolved and only some scattered vessels were seen within the epithelium on en face angiography at the mid-point of treatment. The adjacent subepithelium vessel network at this point appeared denser, instead of the expected decrease (arrowheads). The patient underwent 2 additional cycles of 5-FU which led to clinical and HR-OCT tumor resolution. With lesion resolution, no blood vessels were seen within the epithelium while the subepithelial vascular plexus appeared normalized.

In this patient, tumor metrics including tumor area, tumor volume, tumor depth, and total tumor density decreased with treatment as expected. Similarly, VAD within the OSSN

greatly decreased between the different time points. Interestingly and similar to the previous case, the VAD in the subepithelial tissue adjacent to the tumor increased from presentation (28.45%) to mid-treatment (40.22%), and then decreased with tumor resolution (20.80%). VAD in the subepithelial tissue under the OSSN remained stable between presentation and mid-treatment and then increased with tumor resolution, possibly due to a better unobstructed visualization of the blood vessels. At resolution, subepithelial VAD levels below the resolved tumor (13.14%) were comparable with subepithelial VAD levels in a similar location in the contralateral uninvolved eye (15.98%). (Figure 4).

Case 4 highlighting gradual decrease in the epithelial and subepithelial vascular plexus with tumor resolution.: A 46-year-old female patient presented with a gelatinous conjunctival OSSN located inferior nasally in the right eye and accompanied by multiple abnormal vessels. (Figure 5). HR-OCT confirmed the presence of a thickened, hyperreflective epithelium with abrupt transition from the normal epithelium, classic for OSSN. The epithelial thickness map similarly showed thickening in the area of the tumor. En face angiography imaging revealed blood vessels within the lesion and a dense vascular network in the subepithelial space. Shadowing caused by the tumor nodule blocked visualization of some blood vessels directly beneath the tumor (asterisk). At mid-treatment, after 4 cycles of 5-FU, a small opacity persisted clinically at 8 o'clock. Small areas of slightly thickened, hyperreflective epithelium were seen on HR-OCT around 7:30 to 8 o'clock. By OCTA, blood vessels were dramatically decreased in the epithelium by the mid-point. The subepithelial vascular plexus under and adjacent to the tumor also decreased on en face angiography. After 2 additional cycles of 5-FU, the OSSN appeared resolved clinically and by HR-OCT imaging. The scattered epithelial vessels disappeared and subepithelial vascular plexus further decreased and acquired a normal appearance. The VAD within the OSSN greatly decreased at mid-treatment and was not quantifiable at tumor resolution. In this case, the VAD in the subepithelial tissue under and adjacent to the tumor gradually decreased over the course of treatment. Interestingly, subepithelial VAD in the contralateral uninvolved eye was found to be higher than the VAD in the subepithelial tissue adjacent to the now resolved tumor. (Figure 5).

Case 7 highlighting dramatic decrease in the sea-fan vascular network of tumor epithelium and adjacent subepithelial vascular plexus with tumor resolution. Note improved visualization of the subepithelial vascular plexus as the tumor resolved.: A 69-year-old female presented with a papillomatous and gelatinous OSSN of the left conjunctiva temporally and the cornea from 12 to 6 o'clock with multiple abnormal blood vessels. (Figure 6). HR-OCT images revealed thickened hyperreflective epithelium with abrupt transition, classic features of OSSN. En face angiography imaging revealed a "sea fan" abnormal vascular network within the OSSN. Additionally, 200 um subepithelial to the tumor and in the adjacent subepithelial tissue there was a dense subepithelial vascular network. The patient underwent 2 cycles of 5-FU with dramatic tumor regression seen clinically and by HR-OCT examination. At this midpoint, the angiography images revealed decreasing vascular network within the OSSN. Vessels directly underneath the tumor were initially not visible due to blockage from the thick tumor, but as the tumor was decreasing in thickness, more blood vessels were visible in the subepithelial tissue under the tumor.

5-FU was continued for 6 more cycles, leading to clinical and HR-OCT evidence of tumor resolution. At resolution, en face angiography was void of any blood vessels in the epithelium and the subepithelial blood vessels appeared normalized. Tumor metrics including tumor area, tumor volume, tumor depth, and total tumor density decreased with treatment as expected. In addition, VAD within the OSSN greatly decreased at mid-treatment and was calculated as zero with tumor resolution. In this case, VAD in the subepithelial tissue adjacent to the tumor did not increase but rather remained relatively stable at mid-treatment and then decreased with tumor resolution. Interestingly, the VAD beneath the OSSN gradually increased between the different time-points, likely because as the tumor resolved it allowed for better visualization of the subtumor vascular plexus. At resolution, subepithelial VAD levels below the tumor (19.28%) were comparable with subepithelial VAD levels in a similar location in the contralateral uninvolved eye (21.01%). In this case, post treatment incisional biopsy was performed which confirmed tumor resolution. (Figure 6).

4. Discussion

Tumor microcirculation is highly complex and yet to be completely understood. Initiation of tumor angiogenesis requires the release of chemical signals from tumor cells in a rapid growth phase. This stimulates responsive blood vessels in the tissue surrounding the tumor. (18) Vasculature in neoplastic lesions exhibits functional and structural heterogeneity and has been noted to significantly differ from adjacent unaffected tissue. (19) While normal vasculature is hierarchically organized, tumor vasculature is immature, tortuous and hyperpermeable due to an abnormal basement membrane and diminished muscle cell and endothelial cells. (20) These abnormal vascular networks are thought to be key factors in assisting tumor growth and metastasis. While the above findings have been well described for different types of tumors, the literature on vascular networks of ocular surface tumors is currently limited.

Hence in this study, we utilized OCTA to assess tumor vasculature in 10 individuals with a diagnosis of OSSN that were treated with topical medical therapy. As expected, we found that tumor related metrics including tumor area, tumor volume, tumor depth and total tumor density significantly decreased over time with topical immuno- or chemotherapy. This aligned to what we noted on clinical examination. The novel information provided in this study by the OCTA technology is the quantification of vascular metrics in and around the tumor during treatment. This may provide possible insights into tumor vascular networks, pathophysiology and host response.

Similar to our previous work (16), the VAD at presentation was highest within the tumor, but in that study, we did not evaluate changes with treatment. The purpose of the study was to take this a step further and evaluate the changes with topical chemo and immuno-therapy. We found that VAD within the tumor significantly decreased ($p<0.001$) over treatment, almost completely disappearing with tumor resolution (Table 3). Overall, the VAD in the subepithelial tissue beneath the tumor showed a similar trend, decreasing from presentation to mid-treatment and then remaining relatively stable thereafter. However, in cases of thick tumors (e.g., case 7), the VAD in the subepithelium beneath the OSSN at presentation was

likely under-estimated, due to decreased visibility/blockage of the vessels. In such cases, VAD in the subepithelium beneath the OSSN actually increased with treatment, as tumor resolution allowed for better visualization of the subepithelial vascular plexus. In most cases, the subepithelial VAD beneath the OSSN after tumor resolution was similar to the subepithelial VAD at the same location in the contralateral, unaffected eye, suggesting a normalization of the subepithelial blood vessel density.

In contrast, blood vessels in the subepithelial tissue adjacent to the tumor were not obstructed by the presence of a tumor, thus facilitating VAD calculation. While most tumor metrics decreased over treatment, a more intriguing finding of this study is that the mean VAD in the subepithelial tissue adjacent to the tumor overall increased before decreasing (Table 4). This increase was seen in 50% (5/10) of cases. In some cases (e.g., case 4, 8), VAD in the subepithelial tissue adjacent to the tumor decreased with treatment and in one case, the VAD remained relative stable (e.g., case 10). The decrease from mid to final resolution was significant ($p=0.009$). We examined the relationship between VAD and time to tumor resolution and noted a significant relationship between VAD in the subepithelial area adjacent to the tumor and tumor resolution. This indicates that tumors with higher baseline vascular density adjacent to the tumor required more cycles of treatment for clinical resolution. More studies are needed to further explore these findings.

Finally, we observed not only a change in quantitative density but also in the appearance of the vascular networks. More specifically, with resolution of OSSN lesions, the intraepithelial vessels disappeared. Furthermore, the vascular network of the subepithelial tissue and the adjacent subepithelial tissue appeared less tortuous and more organized and also looked similar to the vascular network of the unaffected eye. Our findings align with the general concept of a chaotic tumor vasculature in neoplasia as we observed irregular and dense vascular plexuses within the tumor at presentation that regressed quantitatively and qualitatively as the tumor responded to topical therapy. We were also able to identify vascular trunks which appeared large in diameter and traveled towards the lesion which may represent feeder vessels in 8 of the 10 lesions. These findings agree with similar data recently published by Binotti et al. (21) In that paper, it was reported that malignant lesions exhibit a greater perilesional vessel diameter and depth, and these vessels may represent feeder vessels. In contrast, it was reported that in 22 patients with benign, pre-invasive and invasive ocular surface tumors, the mean diameter of afferent vessels was smaller than efferent vessels on IGCA. It is important to note that OCTA cannot identify blood flow direction. (10)

Similar findings with respect to changing density and complexity have been seen on biopsy in other cancers. In a small cell lung cancer mouse model (22), cisplatin injected intraperitoneally led to a decrease in vessel density when measured through immunohistochemistry in the entire tumor as compared to pre-treatment. In a rat model of mammary adenocarcinoma (23), treatment with photodynamic therapy and a cysteine protease inhibitor led to decreased vascular network complexity (quantified via fractal dimension (FD) of immunohistochemistry specimens) compared to pre-treatment. Interestingly, OCTA has demonstrated similar changes *in-vivo* in other models. In a murine mammary tumor model (24), intraperitoneal cyclophosphamide (CTX) led to the resolution

of abnormal, disorganized blood vessels networks with the appearance of less complex and more organized vessels when observing OCTA images as well as based on FD (measure of complexity) and lacunarity (measure of homogeneity).

Concerning the ocular surface, one study used ICGA to describe OSSN vascular networks and their changes in 6 patients receiving subconjunctival/perilesional injections of 5-FU. (25) Following the injection therapy with 5-FU, intratumoral and conjunctival feeding vessels vanished in five of the six cases, and patchy ischemic regions were identified in three of the six cases. Similarly, in our study, blood vessels within the tumor completely vanished in all cases by the end of the treatment. Similarly, blood vessels within the subepithelial tissue decreased in density in all cases. These findings reinforce the idea that similar to tumors elsewhere in the body, that normalization of tumor vasculature in OSSN occurs in response to treatment.

Unexpectedly, in some cases we found an initial increase in vascular density in the subepithelial tissue adjacent to the tumor with treatment. The significance of the finding is unclear but several explanations are possible. For example, it has been reported that chemotherapy regimens may induce a cancer-mediated release of cytokines and chemokines which may then generate an inflammatory response or stimulate angiogenesis. (26) 5-FU, in particular, has been shown to increase levels of IL-6 and other inflammatory mediators. (27) The inflammatory response can also cause temporary vasodilation of the subepithelial tissue blood vessels. Dilated blood vessels increase the pixels within the OCTA frame and can affect the VAD calculation. 5-FU associated angiogenesis has also been demonstrated in other tumor models. In mice, circulating endothelial progenitor cell (CEP) numbers rapidly increased (within 24 hours) after a single bolus of 5-FU was injected intraperitoneally. (28) CEPs then populated and integrated into the tumor vasculature in mice with lung carcinoma, potentially linking antitumor therapy with transient angiogenesis. In a breast carcinoma mouse model, intraperitoneal administration of 5-FU led to an initial increase in blood vessel density of tumor samples (imaged via immunofluorescence) taken on day 4 followed by a decrease in vascular density of tumor samples taken on day 8 and a return to baseline levels on day 12. (29) Perhaps a similar effect of 5-FU on blood vessels adjacent to the OSSN tumor may explain the findings noted in our study. Future studies using other treatment medications may further explore this observation.

Our study findings do not come without limitations. First, our cases were diagnosed with OSSN through clinical examination and HR-OCT findings. A biopsy was purposefully not performed as surgical intervention could potentially induce changes in the virgin blood vessel network. However, we have previously published on the high sensitivity and specificity of HR-OCT in assisting in the diagnosis of OSSN. (30) Similarly, resolution was confirmed clinically and by OCT normalization. Second, our results are limited by our sample size, of which only 10 of 30 individuals had the high-quality images necessary to evaluate our metrics of interest. Patient movement created artifact which eliminated several cases. Nevertheless, significance was achieved, suggesting that our sample size was sufficient to detect changes in VAD over time. In addition, thick tumors and leukoplakia precluded detailed visualization of blood vessels especially in the subepithelial tissue in certain cases. Especially in cases of thick tumors, we likely under-estimated the subepithelial

VAD under the OSSN. If so, the change over treatment might in fact be even more dramatic. To counteract this, our measurements were performed in a peripheral area of the tumor where thickness was less than 300 μm, not in the central tumor area. This was done to avoid false negative underestimations of the VAD in the thickened tumor and subepithelial space under the tumor. As technology evolves for better penetration and less shadowing, thicker tumors will potentially be better evaluated. Fourth, as a biopsy was not performed, tumor grade could not be determined. Further studies are needed to examine relationships between baseline and change in vessel characteristics and tumor grade and stage. In a similar manner, further studies examining VAD in individuals without neoplastic conjunctival lesions are needed. Similar to our first study (14), we encountered difficulties with image processing in some cases, including manual segmentation of the tumors, projection artifacts, vascular density calculations. Hopefully these will be minimized in the future as the technology and software improves. Future automation of vascular density calculations will certainly facilitate analysis and increase accuracy in calculations. Lastly, we did not measure variation in the vascular plexus of the contralateral, non-affected eye over time as we did not expect significant changes.

Despite these limitations, this study provides novel information on changes in blood vessel networks within and around OSSN with medical therapy. The OCTA provided insight into the pathophysiology of tumor angiogenesis, describing decreasing epithelial vascular density with tumor resolution and normalization in appearance of subepithelial vascular networks associated with tumor resolution. The finding of increased vascular density at the midpoint of treatment in some cases brings new questions to the understanding of tumor angiogenesis. It is unclear why this occurred in some cases and not in others. Future studies will need to evaluate tumor angiogenesis and how different treatment modalities affect vascular networks.

Acknowledgement:

Despoina Theotoka is a scholar of the Onassis Foundation.

Support:

The Dr. Ronald and Alicia Lepke Grant, the Lee and Claire Hager Grant, the H. Scott Huizenga Grant, the Robert Baer Family Grant, the Emilyn Page and Mark Feldberg Grant, the Robert and Virginia Farr Grant, the Jose Ferreira de Melo Grant, the Calvin and Flavia Oak Support Fund, Richard and Kathy Lesser Grant, the Ted and Michele Kaplan Grant, the Honorable A. Jay Cristol Grant, the Carol Soffer Grant, and the Richard Azar Family Grant Park (institutional grants), Nikolaidis Institution (Dr. Despoina Theotoka), NIH Center Grant P30EY014801, and a grant from the Research to Prevent Blindness (RPB), Guangzhou Science and Technology Project (No.201804010038) (Dr. Zhiping (No.1201581612), and Guangdong Basic and Applied Basic Research Foundation (No. 2020A1515010276) (Dr. Zhiping Liu), The Department of Veterans Affairs, Veterans Health Administration, Office of Research and Development, Clinical Sciences R&D (CSRD) I01 CX002015 (Dr. Galor) and Biomedical Laboratory R&D (BLRD) Service I01 BX004893 (Dr. Galor), Department of Defense Gulf War Illness Research Program (GWIRP) W81XWH-20-1-0579 (Dr. Galor) and Vision Research Program (VRP) W81XWH-20-1-0820 (Dr. Galor), National Eye Institute R01EY026174 (Dr. Galor) and R61EY032468 (Dr. Galor), NIH Center Core Grant P30EY014801 (institutional) and Research to Prevent Blindness Unrestricted Grant (institutional).

6. References

1. Lee GA, Hirst LW. Ocular surface squamous neoplasia. Survey of Ophthalmology. 1995;39(6):429–50. [PubMed: 7660300]

2. Shields CL, Alset AE, Boal NS, Casey MG, Knapp AN, Sugarman JA, et al. Conjunctival Tumors in 5002 Cases. Comparative Analysis of Benign Versus Malignant Counterparts. The 2016 James D. Allen Lecture. American Journal of Ophthalmology. 2017;173:106–33. [PubMed: 27725148]

3. Sayed-Ahmed IO, Palioura S, Galor A, Karp CL. Diagnosis and Medical Management of Ocular Surface Squamous Neoplasia. Expert review of ophthalmology. 2017;12(1):11–9. [PubMed: 28184236]

4. Al Bayyat G, Arreaza-Kaufman D, Venkateswaran N, Galor A, Karp CL. Update on pharmacotherapy for ocular surface squamous neoplasia. Eye and Vision. 2019;6(1):24. [PubMed: 31417938]

5. Ma IH, Hu FR, Wang IJ, Chen WL, Hsu YJ, Chu HS, et al. Clinicopathologic correlation of ocular surface squamous neoplasia from a university hospital in North Taiwan 1994 to 2014. J Formos Med Assoc. 2019;118(4):776–82. [PubMed: 30266199]

6. Shousha MA, Karp CL, Canto AP, Hodson K, Oellers P, Kao AA, et al. Diagnosis of ocular surface lesions using ultra-high-resolution optical coherence tomography. Ophthalmology. 2013;120(5):883–91. [PubMed: 23347984]

7. Nanji AA, Sayyad FE, Galor A, Dubovy S, Karp CL. High-Resolution Optical Coherence Tomography as an Adjunctive Tool in the Diagnosis of Corneal and Conjunctival Pathology. Ocul Surf. 2015;13(3):226–35. [PubMed: 26045235]

8. Tran AQ, Venkateswaran N, Galor A, Karp CL. Utility of high-resolution anterior segment optical coherence tomography in the diagnosis and management of sub-clinical ocular surface squamous neoplasia. Eye Vis (Lond). 2019;6:27. [PubMed: 31463333]

9. Anijeet DR, Zheng Y, Tey A, Hodson M, Sueke H, Kaye SB. Imaging and evaluation of corneal vascularization using fluorescein and indocyanine green angiography. Invest Ophthalmol Vis Sci. 2012;53(2):650–8. [PubMed: 22205599]

10. Brunner M, Romano V, Steger B, Vinciguerra R, Lawman S, Williams B, et al. Imaging of Corneal Neovascularization: Optical Coherence Tomography Angiography and Fluorescence Angiography. Invest Ophthalmol Vis Sci. 2018;59(3):1263–9. [PubMed: 29625447]

11. Lee WD, Devarajan K, Chua J, Schmetterer L, Mehta JS, Ang M. Optical coherence tomography angiography for the anterior segment. Eye Vis (Lond). 2019;6:4. [PubMed: 30775387]

12. Akagi T, Uji A, Huang AS, Weinreb RN, Yamada T, Miyata M, et al. Conjunctival and Intrascleral Vasculatures Assessed Using Anterior Segment Optical Coherence Tomography Angiography in Normal Eyes. Am J Ophthalmol. 2018;196:1–9. [PubMed: 30099035]

13. Roberts PK, Goldstein DA, Fawzi AA. Anterior Segment Optical Coherence Tomography Angiography for Identification of Iris Vasculature and Staging of Iris Neovascularization: A Pilot Study. Curr Eye Res. 2017;42(8):1136–42. [PubMed: 28441067]

14. Liu Z, Karp C, Galor A, Bayyat GJA, Jiang H, Wang J. Role of Optical Coherence Tomography Angiography in the Characterization of Vascular Network Patterns of Ocular Surface Squamous Neoplasia. The Ocular Surface. 2020.

15. Liu Z, Wang H, Jiang H, Gameiro GR, Wang J. Quantitative analysis of conjunctival microvasculature imaged using optical coherence tomography angiography. Eye Vis (Lond). 2019;6:5. [PubMed: 30766893]

16. Liu Z, Karp CL, Galor A, Al Bayyat GJ, Jiang H, Wang J. Role of optical coherence tomography angiography in the characterization of vascular network patterns of ocular surface squamous neoplasia. Ocul Surf. 2020.

17. Perneger TV. What's wrong with Bonferroni adjustments. Bmj. 1998;316(7139):1236–8. [PubMed: 9553006]

18. Farnsworth RH, Lackmann M, Achen MG, Stacker SA. Vascular remodeling in cancer. Oncogene. 2014;33(27):3496–505. [PubMed: 23912450]

19. Pries AR, Cornelissen AJ, Sloot AA, Hinkeldey M, Dreher MR, Höpfner M, et al. Structural adaptation and heterogeneity of normal and tumor microvascular networks. PLoS Comput Biol. 2009;5(5):e1000394. [PubMed: 19478883]

20. Siemann DW. The unique characteristics of tumor vasculature and preclinical evidence for its selective disruption by Tumor-Vascular Disrupting Agents. Cancer Treat Rev. 2011;37(1):63–74. [PubMed: 20570444]

21. Binotti WW, Mills H, Nosé RM, Wu HK, Duker JS, Hamrah P. Anterior segment optical coherence tomography angiography in the assessment of ocular surface lesions. (1937-5913 (Electronic).

22. Frenzel T, Hoffmann B, Schmitz R, Bethge A, Schumacher U, Wedemann G. Radiotherapy and chemotherapy change vessel tree geometry and metastatic spread in a small cell lung cancer xenograft mouse tumor model. PLoS One. 2017;12(11):e0187144. [PubMed: 29107953]

23. Jurczyszyn K, Osiecka BJ, Ziolkowski P. The use of fractal dimension analysis in estimation of blood vessels shape in transplantable mammary adenocarcinoma in Wistar rats after photodynamic therapy combined with cysteine protease inhibitors. Comput Math Methods Med. 2012;2012:793291. [PubMed: 22991578]

24. Kim H, Eom TJ, Kim JG. Vascular morphometric changes during tumor growth and chemotherapy in a murine mammary tumor model using OCT angiography: a preliminary study. Current Optics and Photonics. 2019;3(1):54–65.

25. Sun Y, Hua R. Ocular surface squamous neoplasia: angiographic characteristics and response to subconjunctival/perilesional 5-fluorouracil injections. Drug Des Devel Ther. 2019;13:1323–34.

26. Sanchez LR, Borriello L, Entenberg D, Condeelis JS, Oktay MH, Karagiannis GS. The emerging roles of macrophages in cancer metastasis and response to chemotherapy. J Leukoc Biol. 2019;106(2):259–74. [PubMed: 30720887]

27. Gopinathan G, Milagre C, Pearce OMT, Reynolds LE, Hodivala-Dilke K, Leinster DA, et al. Interleukin-6 Stimulates Defective Angiogenesis. Cancer Res. 2015;75(15):3098–107. [PubMed: 26081809]

28. Shaked Y, Henke E, Roodhart JM, Mancuso P, Langenberg MH, Colleoni M, et al. Rapid chemotherapy-induced acute endothelial progenitor cell mobilization: implications for antiangiogenic drugs as chemosensitizing agents. Cancer Cell. 2008;14(3):263–73. [PubMed: 18772115]

29. Fung AS, Lee C, Yu M, Tannock IF. The effect of chemotherapeutic agents on tumor vasculature in subcutaneous and orthotopic human tumor xenografts. BMC Cancer. 2015;15:112-. [PubMed: 25884767]

30. Nanji AA, Sayyad FE, Galor A, Dubovy S, Karp CL. High-Resolution Optical Coherence Tomography as an Adjunctive Tool in the Diagnosis of Corneal and Conjunctival Pathology. The ocular surface. 2015;13(3):226–35. [PubMed: 26045235]

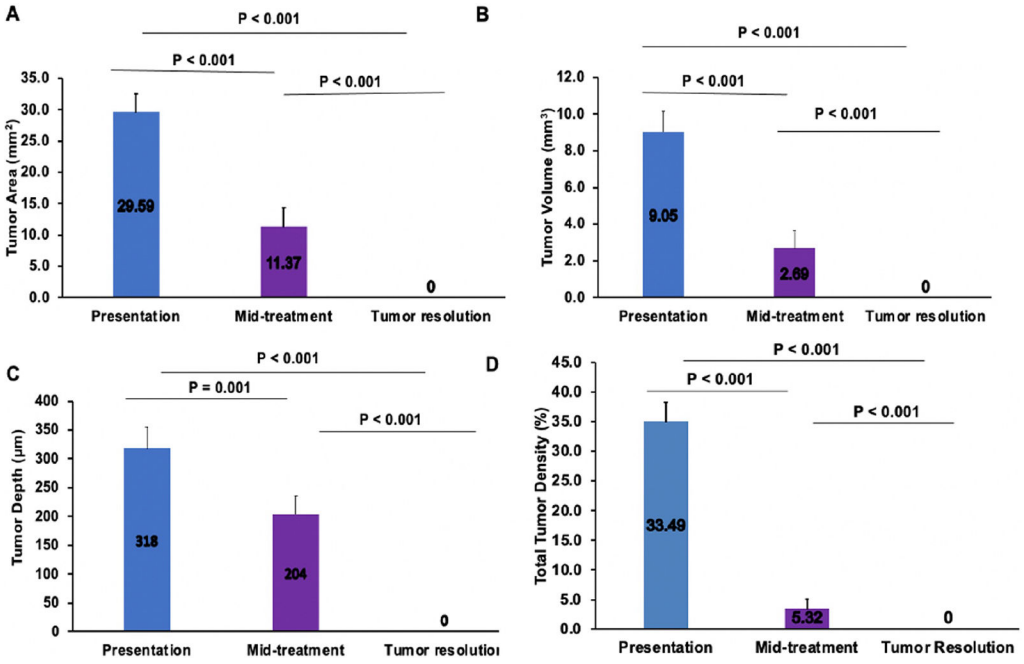

Fig. 1.

Changes of tumor area (A), tumor volume (B), tumor depth (C), and total tumor density (D) at presentation, mid-treatment, and at tumor resolution, all showing statistically significant changes throughout treatment.

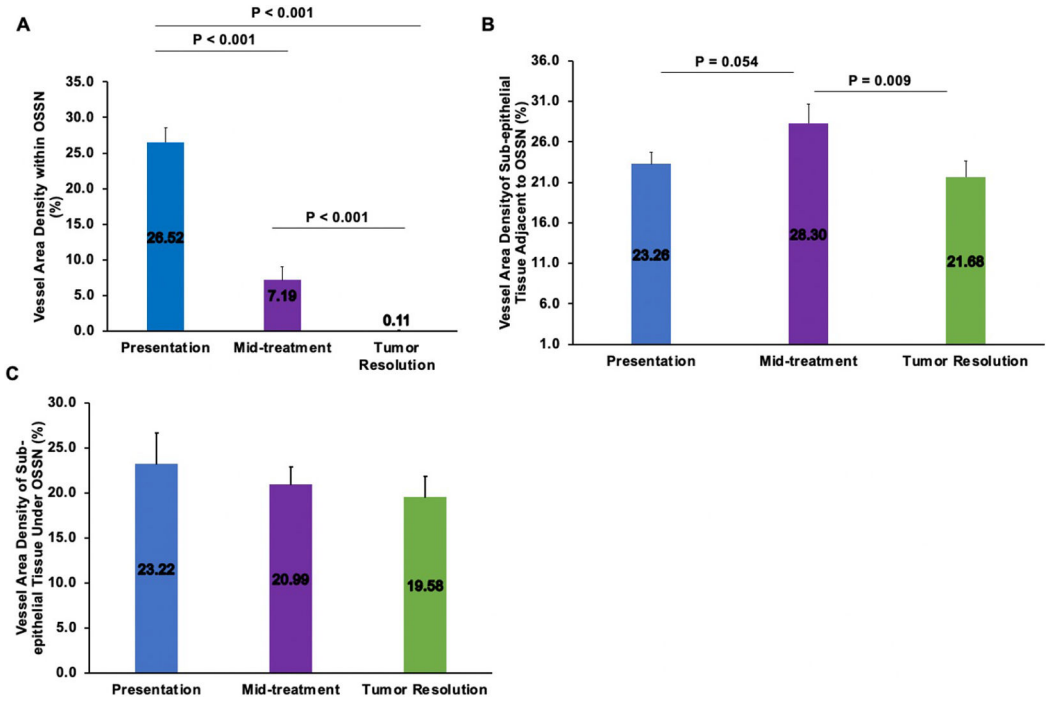

Fig. 2.

Changes in vessel area density within OSSN (A), sub-epithelial tissue adjacent to OSSN (B) and sub-epithelial tissue under OSSN (C) at presentation, mid-treatment and at tumor resolution. OSSN; ocular surface squamous neoplasia.

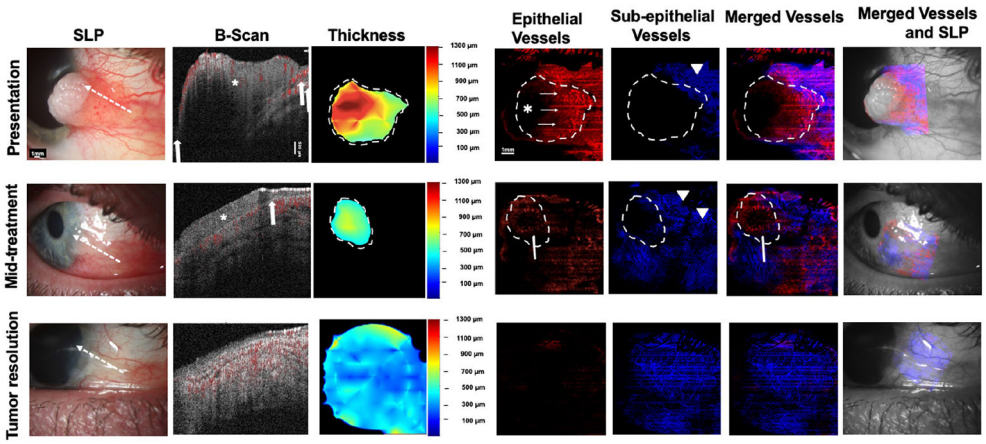

Fig. 3. A 38-year-old male presenting with a leukoplakic and papillomatous OSSN (Case 1). SLP: At presentation, a leukoplakic and papillomatous OSSN from 2 to 4 o'clock with intrinsic vascularity and feeder vessels is seen. At mid-treatment, after 2 cycles of 5-FU and 3 cycles of MMC, the leukoplakic component resolved while the papillomatous remains. Conjunctiva hyperemia is seen. At tumor resolution, there is some remaining mild hyperemia. White dashed arrow shows cross-sectional cut of OCT. **B-scan images:** At presentation, a thickened, hyperreflective epithelium (asterisk) with abrupt transition (arrows) and significant posterior shadowing is seen. Blood flow (shown in red color) within the superficial part of the tumor as well as in the adjacent subepithelium is noted. Shadowing limits visualization of some blood flow within and below the tumor. At mid-treatment, thickened, hyperreflective epithelium (asterisk) with abrupt transition (arrows) is improved but persists. Blood flow is seen within the tumor as well as in the subepithelium. At tumor resolution, thin avascular epithelium and blood flow in the subepithelium is seen. **Thickness map:** Changes in the thickness of the tumor are shown at presentation, mid-treatment, and at tumor resolution. Dashed white lines indicate the tumor boundary. Note highly elevated tumor head at presentation (red) which corresponds to areas of blockage of vessel visibility. **Enface angiograph of epithelial vessels:** At presentation, dense BV (white thin arrows) are seen within the papillomatous part/tail of the OSSN. Straight horizontal lines represent artifacts from patient movement. Leukoplakia prevents visualization of BV at that corresponding thick part of the tumor (asterisk). At mid-treatment, "sea-fan" BV (white arrow) are seen within the remaining papillomatous head of the OSSN and at tumor resolution epithelium appears to be grossly avascular. Dashed white lines indicate the tumor boundary. Enface angiograph of the subepithelial vessels (200 μm): At presentation, dense BV are seen in the subepithelium at the OSSN edge and adjacent to it (arrowhead). Shadowing precluded full visualization of BV directly under the tumor at presentation. At mid-treatment, BV increased in the area adjacent to the tumor (two arrowheads). At tumor resolution BV appear decreased and more regular , similar to the contralateral eye. Dashed white lines indicate the tumor boundary. **Merged vessels:** The tumor BV (red) and sub-epithelial BV angiographies (blue) were merged at presentation, mid-treatment and at tumor resolution. Note "sea-fan" visible (arrow) at mid-treatment. Dashed white lines indicate the tumor boundary. **Merged vessels and SLP:** Overlay of the enface angiograph with grayscale slit-lamp at presentation, mid-treatment and at tumor resolution.OSSN;

ocular surface squamous neoplasia, SLP; slit lamp photograph, OCT; optical coherence tomography, BV; blood vessels.

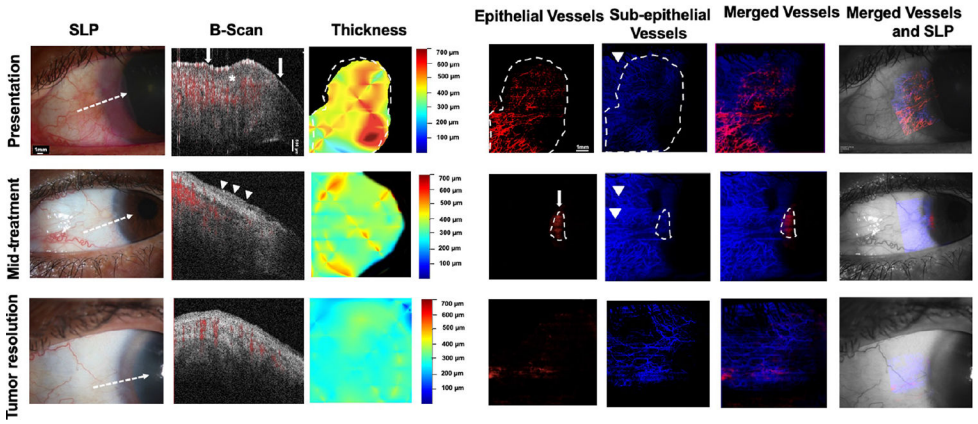

Fig. 4. A 60-year-old woman presenting with a gelatinous OSSN involving the nasal limbus of the left eye (Case 3).SLP:

A corneal and limbal gelatinous OSSN from 6 to 12 o'clock nasally in the left eye with multiple BV is seen at presentation. At mid-treatment, after 4 cycles of 5-FU, the tumor is dramatically improved, but some opalescence and gelatinous changes persist from 8 to 9 o'clock. Normal conjunctiva is seen at tumor resolution. White dashed arrow shows cross-sectional cut of OCT. **B-scan images:** At presentation, a thickened, hyperreflective epithelium (asterisk), with abrupt transition (arrows) is seen. Blood flow within part of the corneal and conjunctival epithelium as well as in the subepithelium is noted (shown in red). At mid-treatment, greatly normalized epithelium with a focal area of slightly thickened, hyperreflective epithelium is seen in the conjunctiva (arrowheads). Blood flow signals in the subepithelium is seen. At tumor resolution, epithelium is avascular and thin and blood flow is noted only in the subepithelium. **Thickness map:** Changes in the thickness of the tumor are shown at presentation, mid- treatment, and at tumor resolution. Dashed white lines indicate the tumor boundary. **Enface angiograph of epithelial vessels:** Dense BV within the cornea and conjunctiva are seen at presentation, resolving at mid-treatment with some BV remaining at the cornea (white arrow) and disappearing at tumor resolution. Dashed white lines indicate the tumor boundary. **Enface angiograph of the subepithelial vessels (200 μm):** Dense BV are seen at presentation (arrowhead) which appear denser and complex at mid-treatment adjacent to the tumor (arrowheads). At tumor resolution, subepithelial BV have decreased and acquired a more regular appearance and were quantitatively and qualitatively similar to the uninvolved contralateral eye. Dashed white lines indicate the tumor boundary. **Merged vessels:** The tumor vessels (red) and sub-epithelial BV angiographies (blue) were merged at presentation, mid-treatment, and at tumor resolution. Dashed white lines indicate the tumor boundary. **Merged vessels and SLP:** Overlay of the enface angiograph with grayscale slit-lamp at presentation, mid-treatment, and at tumor resolution. OSSN; ocular surface squamous neoplasia, SLP; slit lamp photograph, OCT; optical coherence tomography, BV; blood vessels.

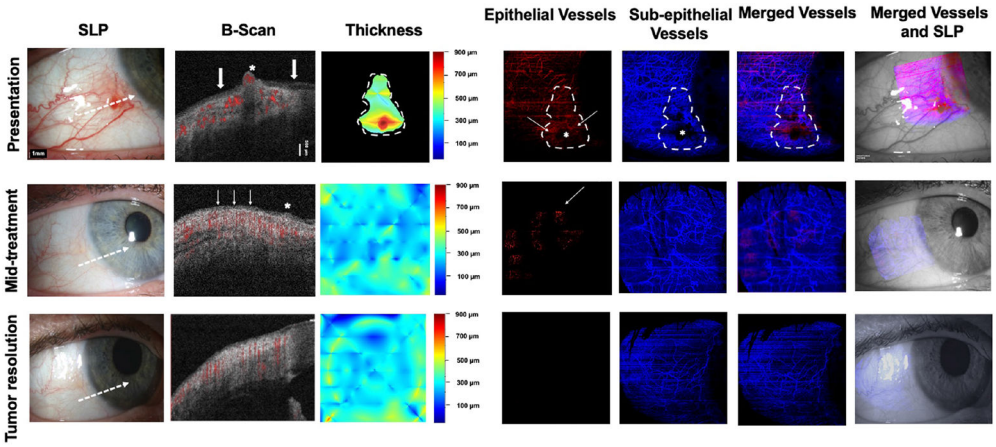

Fig. 5. A 46-year-old female presenting with a gelatinous OSSN of the right eye (Case 4).SLP: At presentation, a conjunctival gelatinous OSSN is seen inferior temporally with feeder vessels. At mid-treatment, after 4 one week cycles of 5 FU, the tumor is greatly improved. After another 2 cycles of 5-FU, conjunctiva appears normal. **White dashed arrow shows cross-sectional cut of OCT. B-scan images:** At presentation, a thickened, hyperreflective epithelium (asterisk), with abrupt transition (arrows) is noted. There is blood flow within the tumor and in the subepithelium (shown in red). At mid-treatment, small areas of slightly thickened, hyperreflective epithelium (asterisk and thin white arrows) remain around 7:30 to 8 o'clock. Blood flow is seen in the subepithelium. At tumor resolution, the epithelium is thin and avascular. Blood flow is noted in the subepithelium only. **Thickness map:** Changes in the thickness of the tumor are shown at presentation, mid-treatment, and at tumor resolution. Note thickened epithelium at presentation which resolved with treatment. Dashed white lines indicate the tumor boundary. **Enface angiograph of epithelial vessels:** A vascular network is seen at presentation (thin white arrows) however the tumor nodule blocks complete visualization of BV at that corresponding area (asterisk). At mid-treatment, there is significant decrease in the epithelial BV with one BV remaining (white thin arrow) and at tumor resolution, all of the epithelium appears avascular. Horizontal lines represent artifacts. Dashed white lines indicate the tumor boundary. **Enface angiograph of the subepithelial blood vessels (200 μm):** Dense BV are seen at presentation. Focal shadowing from the tumor nodule blocks visualization of the respective BV (asterisk). At mid-treatment, BV have decreased. As the tumor has also decreased in size, there is no longer shadowing and all subepithelial BV are now visualized. At tumor resolution, BV have further decreased and appear normalized. Dashed white lines indicate the tumor boundary. **Merged vessels:** The tumor BV (red) and sub-epithelial BV angiographies (blue) were merged at presentation, mid-treatment, and at tumor resolution. Dashed white lines indicate the tumor boundary. **Merged vessels and SLP:** Overlay of the enface angiograph with grayscale slit-lamp at presentation, mid-treatment and at tumor resolution. OSSN; ocular surface squamous neoplasia, SLP; slit lamp photograph, OCT; optical coherence tomography, BV; blood vessels.

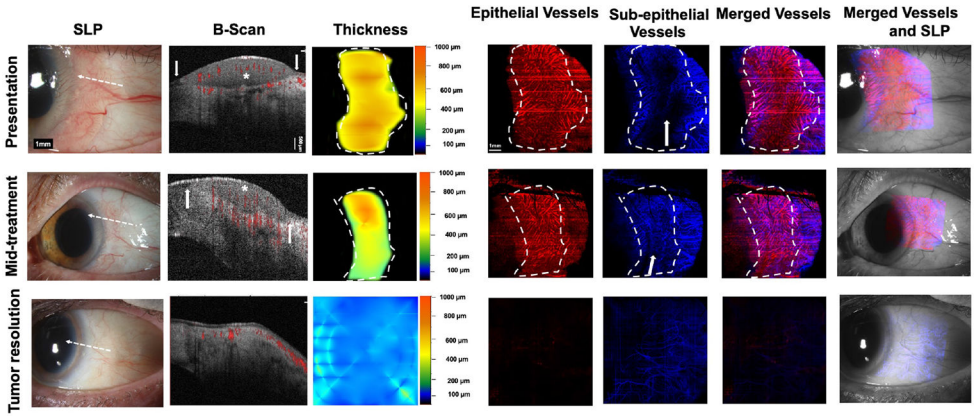

Fig. 6. A 69-year-old woman presenting with a gelatinous and papillomatous OSSN of the left eye (Case 7). SLP:

A gelatinous and papillomatous OSSN of the conjunctiva encroaching on the cornea temporally from 12 to 6 o'clock in the left eye with intrinsic vascularity and feeder vessels is seen at presentation. At mid-treatment, after 2 cycles of 5-FU, the gelatinous and papillomatous OSSN has dramatically decreased in size. At tumor resolution, the conjunctiva appears normal while some opacity (consistent with scar) remains in the cornea temporally. White dashed arrow shows cross-sectional cut of OCT. **B-scan images:** At presentation, thickened hyperreflective epithelium (asterisk) with abrupt transition (arrows) is seen. Blood flow (shown in red) within the tumor as well as in the subepithelium is noted. Some shadowing limits complete blood flow visualization under the tumor. At mid-treatment, the flow in the epithelium and subepithelium is still present. At tumor resolution, thin epithelium is noted and blood flow in subepithelium is normalized. **Thickness map:** Changes in the thickness of the tumor are shown at presentation, mid-treatment, and at tumor resolution. Dashed white lines indicate the tumor boundary. **Enface angiograph of epithelial vessels:** Dense BV in a "sea fan" pattern seen at presentation, decreasing at mid-treatment and disappearing at tumor resolution. Straight horizontal lines represent artifacts due to patient movement. Dashed white lines indicate the tumor boundary. **Enface angiograph of the subepithelial vessels (200 μm):** Dense BV at and adjacent to the tumor edge are seen at presentation. Complete visualization of BV immediately underneath the tumor is blocked due to the thick size of the tumor. At mid-treatment, BV adjacent to the tumor appear similar to presentation. In the contrary, BV immediately beneath the tumor are now more visible as the tumor is decreasing in thickness. With tumor resolution, BV adjacent to the tumor and immediately beneath the tumor disappeared. At resolution, subepithelial VAD levels below the tumor were comparable with subepithelial VAD levels in a similar location in the contralateral uninvolved eye. Dashed white lines indicate the tumor boundary. **Merged vessels:** The tumor BV (red) and subepithelial BV angiographies (blue) were merged at presentation, mid-treatment and at tumor resolution. Dashed white lines indicate the tumor boundary. **Merged vessels and SLP:** Overlay of the enface angiograph with grayscale slit-lamp at presentation, mid-treatment and at tumor resolution, showing gradual resolution of the epithelial vasculature and normalization of the subepithelial BV.OSSN; ocular surface squamous neoplasia, SLP; slit lamp photograph, OCT; optical coherence tomography, BV; blood vessels.

Table 1:

Patient characteristics with ocular surface squamous neoplasia

Case #	Sex	Age (years)	Eye	LC	Conjunctiva			Cornea	Treatment	Outcome	P	M	TR
					P	G	L						
1	M	38	OD	N	+	-	+	+	5-FU, MMC	Resolution	+	+	+
2	M	56	OS	N	−	+	−	+	5-FU, IFN α-2b	Resolution	+	+	+
3	F	60	OS	N	−	+	−	+	5-FU	Resolution	+	+	+
4	F	46	OD	T	−	+	−	−	5-FU, MMC	Resolution Neg post Tx Bx	+	+	+
5	M	70	OS	T	−	+	−	+	5-FU	Resolution	+	+	+
6	M	79	OD	N	−	+	−	+	5-FU	Resolution	+	+	+
7	F	69	OS	T	+	+	−	+	5-FU	Resolution Neg post Tx Bx	+	+	+
8	M	66	OS	N	−	+	−	−	5-FU	Resolution Neg post Tx Bx	+	+	+
9	M	46	OD	T	−	+	+	+	5-FU	Resolution	+	+	+
10	M	84	OD	T	−	+	−	+	5-FU	Resolution	+	+	+

LC; location, LKNV; length of corneal neo-vessel invasion, F; female, M; male, OS; left eye, OD; right eye, P; papillary, G; gelatinous, L; leukoplakic, T; temporal, N; nasal, S; superior, 5-FU; 5-fluorouracil, MMC; mitomycin, IFN α-2b; Interferon α-2b, P; presentation, M; mid-treatment, TR; tumor resolution, Neg post Tx Bx; Negative post treatment biopsy.

Table 2:

Tumor area, tumor volume, tumor depth, total tumor density values measured at presentation, mid-treatment and tumor resolution.

Case #	TA-P (mm^2)	TV-P (mm^3)	TD-P (μm)	TTD-P (%)	TA-M(mm^2)	TV-M (mm^3)	TD-M (μm)	TTD-M (%)	TA-TR (mm^2)	TV-TR (mm^3)	TD-TR (μm)	TTD-TR (%)
1	25.77	14.68	569.77	25.60	15.13	4.04	267.33	1.98	0	0	0	0
2	36.92	6.61	179.13	25.8	NA	NA	NA	NA	0	0	0	0
3	38.03	8.9	234.10	34.9	NA	NA	NA	NA	0	0	0	0
4	14.1	3.4	241.27	38.1	NA	NA	NA	NA	0	0	0	0
5	20.42	7.02	343.82	38	10.55	1.8	170.39	5.38	0	0	0	0
6	36.23	12.13	334.91	58.8	NA	NA	NA	NA	0	0	0	0
7	37.11	13.33	359.28	35.2	23.07	6.76	293.14	9.39	0	0	0	0
8	20.89	7.75	370.90	36	10.06	1.24	123.40	4.55	0	0	0	0
9	41.67	7.45	178.47	20.47	1	0.12	115.88	NA*	0	0	0	0
10	24.78	9.18	370.47	22.1	8.43	2.16	256.35	NA*	0	0	0	0

TA; tumor area, TV; tumor volume, TD; tumor depth, TTD; total tumor density, P; presentation, M; mid-treatment, TR; tumor resolution, NA; unable to calculate due to small tumor size, NA*; unable to calculate due to keratinization.

Table 3:

Changes in VAD within the OSSN measured at presentation, mid-treatment and at tumor resolution. P<0.001

VAD within the OSSN	Presentation	Mid-treatment	Tumor resolution
1	21.80	1.94	0.02
2	28.80	8.65	0.00
3	24.64	5.63	1.09
4	22.88	4.73	0.00
5	34.82	2.10	0.00
6	39.90	2.71	0.00
7	28.79	19.62	0.00
8	25.97	15.37	0.00
9	18.01	6.01	0.00
10	19.68	5.10	0.02

VAD; vessel area density, OSSN; ocular surface squamous neoplasia

Table 4:

Changes in VAD in subepithelium adjacent to the OSSN measured at presentation, mid-treatment and at tumor resolution.

VAD in the subepithelium adjacent to the OSSN	Presentation	Mid-treatment	Tumor resolution
1	17.51	37.03	16.54
2	22.04	18.25	18.38
3	28.45	40.22	20.80
4	31.15	29.96	17.89
5	18.39	33.07	33.56
6	17.93	28.69	30.54
7	24.68	24.59	16.40
8	22.95	17.14	16.53
9	26.00	39.11	20.61
10	25.97	24.73	24.62

VAD; vessel area density, OSSN; ocular surface squamous neoplasia